Limnol. Oceanogr., 55(1), 2010, 354–364

In situ measurements of turbulence in fish shoals

Andreas Lorke[a,b*] and W. Nikolaus Probst[a]

[a] Limnological Institute, University of Konstanz, Konstanz, Germany
[b] Institute for Environmental Sciences, University of Koblenz-Landau, Landau, Germany

Abstract

Turbulence was measured in situ within shoals of juvenile perch *Perca fluviatilis* with a self-contained autonomous microstructure profiler near an artificial reef in Lake Constance, Germany. Depth-averaged dissipation rates of turbulent kinetic energy (TKE) correlated with the density of shoaling fish, providing evidence for fish-induced turbulence in a large and stratified lake. The observed range and the depth-averaged values of TKE dissipation rates associated with fish-generated turbulence were comparable with magnitudes of turbulence typically caused by internal waves or wind forcing. Enhanced turbulence within fish shoals could only be observed during periods of low background turbulence and high fish abundance. The observed rates of dissipation of TKE are about two orders of magnitude smaller than production rates of TKE estimated from empirical models on the basis of observed fish size and swimming speed.

The role of biologically generated turbulence for vertical mixing of the ocean became the issue of a recent debate (Kunze et al. 2007; Visser 2007*a*,*b*). Although this issue is not really a new one, it was brought into focus by a study of Kunze et al. (2006), who observed strongly increased levels of turbulence during the ascent of dense swarms of krill performing diel vertical migration in the coastal ocean. These observations led the authors to hypothesize that biologically generated turbulence may affect vertical mixing and marine biogeochemical fluxes on a global scale. This hypothesis is questioned by Visser (2007*a*) with the argument that although marine animals might contribute to the production of turbulent kinetic energy (TKE), owing to low mixing efficiency, their contribution to vertical mixing may be rather weak. Experimental support for the argument raised by Visser et al. (2007*a*) was provided recently by Gregg and Horne (2009), who observed strongly increased rates of TKE dissipation in combination with decreased mixing efficiencies within patches of enhanced acoustic backscatter, most likely caused by small fish.

The observations of Kunze et al. (2006) and Gregg and Horne (2009) are in accordance with an empirical study of Huntley and Zhou (2004), who analyzed the production rates of TKE for marine animals ranging in size from zooplankton to whales and concluded that for schooling animals, regardless of animal size, the magnitude of biologically induced turbulence is comparable with rates of turbulent energy dissipation caused by major storms. In a different approach, on the basis of global estimates of primary production and different methods for quantifying the flux of the produced chemical energy into mechanical energy at higher trophic levels by animal swimming, Dewar et al. (2006) also concluded that the marine biosphere may contribute to mechanical energy in the aphotic ocean at a rate comparable with wind and tidal inputs.

The main reasons for locomotion in habitats with only weak background currents are feeding (Neumann et al. 1996; Schmidt-Nielsen 1997; Cech and Kubecka 2002), predator avoidance (Allouche and Gaudin 2001), and social interaction (Hoare et al. 2000; Behrmann-Godel et al. 2006). For swimming animals, the costs of locomotion are determined not only by the drag force and by the generation of TKE, but also by the intensity of background turbulence in the ambient water. For fish the effect of turbulence on the energetic costs is twofold: On one hand, laboratory studies have demonstrated that ambient turbulence can increase the cost of locomotion (Enders et al. 2003). On the other hand, several recent studies show that fish can also reduce locomotory costs by exploiting vortices generated by water moving past physical structures, by propulsive movements of other fishes (Liao 2007), or even by themselves (Triantafyllou et al. 2000). Further, turbulence affects encounter rates with predators and prey, fish diet composition, feeding behavior, and prey patchiness in a complex way (Mackenzie 2000; Lewis and Pedley 2001). Pitchford et al. (2003), e.g., have demonstrated with mathematical models that in a patchy turbulent environment it is optimal for foraging fish to maintain swimming activity within patches of prey until a threshold of background turbulence is exceeded. Above this turbulence threshold, swimming ceases to be energetically favorable.

Thus, the production of TKE by swimming aquatic animals is an important issue from both the physical and biological point of view. Surprisingly enough, not much is known about turbulence production and dissipation rates in animal schools in their natural environment. Hydrodynamic (Anderson et al. 2001; Drucker and Lauder 2002; Liao 2007) as well as metabolic studies (Wardle et al. 1996; Enders et al. 2003; Nikora et al. 2003) are limited to individual fish or small groups of fish that were forced to swim against artificial flows in laboratory flumes. Within natural habitats, however, interaction between fish swimming behavior and turbulence has rarely been explored.

Here we present direct turbulence measurements in fish shoals within their natural environment. By combining

* Corresponding author: lorke@uni-landau.de

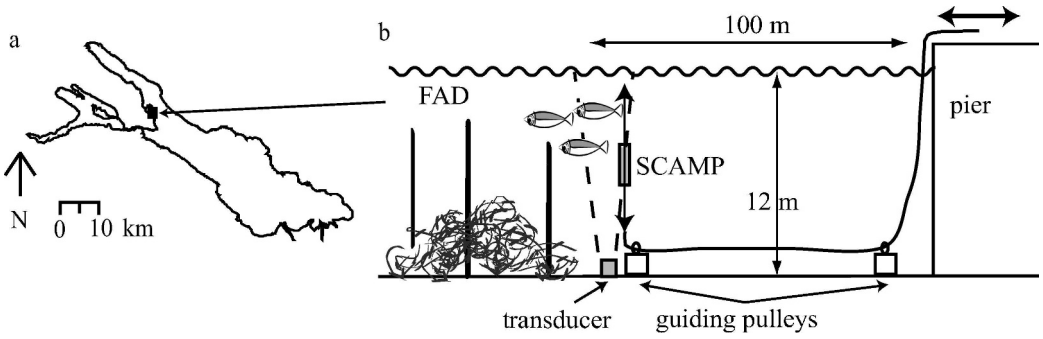

Fig. 1. (a) Map of Lake Constance and location of the study site and (b) experimental setup near the fish aggregation device (FAD, figure not to scale). A mounting holding the SCAMP and the hydroacoustic transducer was installed at 12-m depth on the lake floor northeast of the FAD. Vertical operation of the temperature microstructure profiler (SCAMP) was controlled from the pier using a tether line and two guiding pulleys. Dashed lines indicate the acoustic beam of the transducer.

temperature microstructure measurements with hydroacoustic, gill net, and video-sampling techniques, we estimated dissipation rates of TKE in aggregations of juvenile perch *Perca fluviatilis* L. in the vicinity of an artificial reef in Lake Constance. Our measurements indicate a significant relationship between water column turbulence and fish abundance. In the Discussion section, we present analyses of production rates of TKE by swimming fish using a hydrodynamic and a metabolic approach, and thereby show that the observed effect of fish swimming on water column turbulence is below the range of TKE production rates predicted by these empirical models.

Methods

Study site and experimental setup—Lake Constance is a large, oligotrophic lake with 536 km^2 surface area and 254 m maximum depth (Mürle et al. 2004). The littoral zone, where water depth is less than 10 m, covers about 15% of the lake's surface area and is habitat of many fish species. The most common species in the littoral zone of Lake Constance are perch *P. fluviatilis*, bleak *Alburnus alburnus*, ruffe *Gymnocephalus cernuus*, and dace *Leuciscus leuciscus* (Reyjol et al. 2005). Because the littoral zone is void of three-dimensional bottom structures at most places, artificial reefs, also called fish aggregations devices (FAD), have been installed and maintained by local fishermen for several centuries (Löffler 1997). FAD consist of several vertical poles of 3- to 7-m length rammed into the soft lake bottom. The poles delimit a rectangular base area of approximately 50 to 100 m^2 (7×7 m to 10×10 m base dimensions) on the lake bottom on which a layer of coarse wooden debris is piled up. The height of the brushwood layer may vary between 2 and 7 m. Such artificial reefs are not uncommon in lakes (Prince and Maughan 1978; Bassett 1994; Rogers and Bergersen 1999) because they provide a complex habitat structure. Particularly young fish are assumed to find shelter from predation and take advantage of increased foraging opportunities, as FAD also aggregate benthic fauna that relies on hard substrata for settlement (e.g., bivalves such as *Dreissena polymorpha* and associated gammarids).

While the majority of juvenile fish inhabits the shallowest areas of the littoral zone during spring and summer (Fischer and Eckmann 1997; Stoll et al. 2008), young-of-the-year perch and ruffe are known to aggregate in dense shoals around FAD in late summer and autumn before migrating to the profundal zone of the lake for overwintering (Wang and Eckmann 1994; Lorke et al. 2008).

Measurements were carried out in immediate vicinity of a FAD situated near the marina of Konstanz-Egg (Fig. 1) during autumn aggregation of juvenile perch between August and October 2008. A hydroacoustic transducer was deployed on a bottom-resting mounting at 12-m depth in front of the FAD. The transducer was connected to a scientific echosounder and data acquisition computer installed on a pier, about 100 m away from the FAD. The bottom-resting mounting also supported the vertical operation of a turbulence profiler, which was operated manually from the pier using a tether line and a set of guiding pulleys (Fig. 1). Whenever the tether line was released at the pier, the positively buoyant instrument ascended to the water surface, while recording a temperature microstructure profile. After completing a profile, the instrument was pulled back to the bottom using the tether line. This setup ensured that the microstructure profiler was within the acoustic beam of the transducer, allowing for simultaneous observation of fish and the vertical position of the turbulence profiler throughout the entire water column. Between 10 and 17 temperature microstructure profiles were measured respectively during 15 deployments lasting between 77 and 142 min (Table 1). The length of the individual deployments was limited by battery power of the microstructure profiler. A holding time of at least 5 min at the bottom was used before each microstructure profile to allow profiler-induced turbulence to decay or be advected.

Most of the deployments were accompanied by video observations using a small camera mounted on the turbulence profiler. Fish were sampled using gill nets deployed less than 5 m from the FAD on five sampling days.

Temperature microstructure and video—Temperature microstructure was measured using the self-contained autonomous microstructure profiler (SCAMP, Precision

Table 1. Summary of SCAMP deployments with date, time, and total number of SCAMP profiles measured. Fish abundance is given as minimum–maximum and (mean) values. Depth- and ensemble-averaged dissipation rates of TKE are provided for each deployment. Mean dissipation with fish refers to the ensemble average of profiles, where fish were present during the ascent of SCAMP and mean dissipation without fish refers to profiles in which fish were definitively absent during profiling. Numbers in parentheses are the respective numbers of observation (profiles). Bold indicates the period of high fish abundance, which was included into general linear model (GLM) analysis summarized in Table 4.

Date	Time (hh:mm)	No. of SCAMP profiles	Fish abundance during profiling (m^{-3})	Mean dissipation rate with fish (W kg^{-1})	Mean dissipation rate without fish (W kg^{-1})
25 Aug 2008	15:41–17:33	13	0–0.3(0.2)	1.1×10^{-8}(10)	1.3×10^{-8}(2)
02 Sep 2008	15:12–16:29	10	0–0.5(0.2)	2.6×10^{-8}(10)	—(0)
02 Sep 2008	17:24–19:38	16	0–0.2(0.1)	5.5×10^{-9}(5)	4.7×10^{-9}(10)
09 Sep 2008	08:06–09:54	14	0–0.1(0.0)	6.9×10^{-9}(8)	8.3×10^{-9}(4)
09 Sep 2008	16:05–18:27	16	0–0.5(0.2)	7.2×10^{-9}(9)	—(0)
11 Sep 2008	08:56–11:15	17	0–1(0.6)	1.9×10^{-8}(13)	4.2×10^{-9}(1)
11 Sep 2008	13:04–15:18	18	0–1(0.6)	3.4×10^{-9}(14)	—(0)
11 Sep 2008	16:26–18:40	18	0–1(0.7)	4.0×10^{-9}(17)	2.0×10^{-9}(1)
29 Sep 2008	**15:07–17:15**	**16**	**0–3(0.4)**	**9.2×10^{-10}(6)**	**5.1×10^{-10}(10)**
02 Oct 2008	**09:40–11:18**	**11**	**0–8(0.8)**	**9.5×10^{-9}(6)**	**5.1×10^{-9}(2)**
07 Oct 2008	**08:18–10:32**	**17**	**0–3(0.1)**	**4.1×10^{-9}(5)**	**4.1×10^{-9}(11)**
08 Oct 2008	**08:48–11:03**	**17**	**0–8(3.5)**	**3.3×10^{-9}(12)**	**1.5×10^{-9}(2)**
08 Oct 2008	**14:00–15:21**	**10**	**0–7(3.5)**	**3.5×10^{-9}(7)**	**9.7×10^{-10}(3)**

Measurement Engineering). The instrument measures temperature, the time derivative of temperature, and depth at a rate of 100 Hz, while freely ascending through the water column at a buoyancy-adjusted speed of about 0.1 m s^{-1}. The instrument resolves the vertical temperature profile and temperature fluctuations with a spatial resolution of approximately 1 mm. Data recording and power supply are internal.

Small-scale temperature fluctuations in a temperature-stratified water column are caused by turbulent motions. The intensity of turbulence in terms of the dissipation rate of TKE can be estimated by fitting the observed wave number spectrum of temperature or temperature gradient fluctuations to its theoretical form provided by Batchelor (1959) for homogeneous and isotropic turbulence. In particular, this method is based on estimating the Batchelor cutoff wave number, at which molecular diffusion balances the production of small-scale temperature variance by turbulent stirring and straining of the mean vertical temperature gradient. The Batchelor wave number is a function of the TKE dissipation rate (Batchelor 1959). Temperature microstructure measurements are a common approach for quantifying turbulence and turbulent mixing, particularly in the low-energetic environment of lakes and reservoirs (Imberger and Ivey 1991; Lorke et al. 2003; Hondzo and Haider 2004). Dissipation rates of TKE ε were estimated for profile segments of 0.5-m length by applying a maximum-likelihood fitting technique (Ruddick et al. 2000) on the respective temperature gradient spectra.

Videos from a small waterproof surveillance camera mounted to the upper part of SCAMP were recorded in black and white with a resolution of 756 × 512 pixels using a digital video recorder mounted at the lower end of the instrument. Video recordings are not available for all deployments and profiles because of recorder malfunction and battery depletion, respectively.

Hydroacoustic fish observations—The abundance, size, and swimming speed of fish were measured with a stationary fixed upward-pinging split-beam transducer (E120-7C, SIMRAD) and a scientific echosounder (EY500, SIMRAD). The transducer was operated at 120 kHz, a ping rate ranging between 3 and 10 s^{-1}, a power output of 63 W, and 12 kHz bandwidth. A short pulse length of 0.1 ms was used to obtain a maximum resolution of individual fish within dense fish aggregations.

The abundance of fish was determined between 2- and 6-m depth 30 s before each release of SCAMP. Fish abundance was determined as volume density by scaling the volume backscatter coefficient (S_V) by the target strength (*TS* in dB) distribution (Simmonds and Maclennan 2005; Balk and Lindem 2006). Total length–frequency (*TL-F*) distributions of fish observed in the echogram were estimated by converting the *TS* of tracked fish into *TL* (mm) using:

$$TL = 10^{\left(\frac{TS+116.17}{34.504}\right)} \quad (1)$$

The two parameters in the above equation (116.17 and 35.504) were obtained by linear regression of the observed peaks in the *TS-F* distribution and the peak *TL* of the frequency distribution of the net catches on 08 October 2008 (*see* below).

Tracks of individual fish were analyzed using the automatic tracking routine of SONAR5_Pro, a freeware program provided by Helge Balk (University of Oslo, http://www.fys.uio.no/~hbalk/sonar4_5/Downloads.htm). Tracking criteria were set to a minimum number of 10 single-echo detections (SED), a maximum gap of two pings between consecutive echoes, a vertical gating of 0.1 m, and a minimum mean *TS* of −58 dB. The noise threshold was set to −60 dB. Average swimming speed of individual fish was calculated from a set of 1604 fish tracks recorded between 29 September 2008 and 08 October 2008.

Table 2. Summary of gill net catches. Catch per unit effort (CPUE) was calculated as the number of caught fish per m^2 of net area and hour (h) of exposure. Bold indicates time periods of high fish abundance.

Date	Exposure time (h)	Species	No. caught	CPUE (No. fish h^{-1} m^{-2})
02 Sep 2008	7	Perch	8	0.4
		Ruffe	8	0.4
09 Sep 2008	4.5	Perch	17	0.8
		Ruffe	0	0
11 Sep 2008	10.75	Perch	1	0.1
		Ruffe	4	0.2
29 Sep 2008	**18**	**Perch**	**95**	**4.3**
		Ruffe	**1**	**0.1**
		Roach	**3**	**0.1**
08 Oct 2008	**9**	**Perch**	**106**	**4.8**
		Ruffe	**1**	**0.1**

Net sampling—Fish were sampled with a multimesh gill net set consisting of five net blades with 6-, 9-, 12-, 15-, and 20-mm mesh size (knot to knot) connected in a random order. The net blades with the according mesh size had the following lengths, heights, and catch areas, respectively: 6 mm: 2 m × 1.5 m (3 m^2); 9 mm: 1.8 m × 1.7 m (3.1 m^2); 12 mm: 4 m × 1.6 m (6.4 m^2); 15 mm: 4 m × 1.6 m (6.4 m^2); and 20 mm: 2 m × 1.6 m (3.2 m^2). Gill nets were deployed on five occasions from the morning before the first SCAMP deployment until the late afternoon or dusk after the last SCAMP deployment, respectively (Table 2). The net was set 1 m above the lake bottom perpendicular to the shore covering a depth range between 4 and 12 m. Fish species composition, total length (*TL*), and wet weight (*WW*) of each caught fish was recorded to obtain *TL-F* and *WW-F* distributions. Major size groups of fish were determined from the *TL-F* distributions obtained from net sampling and from hydroacoustic observations using a modal progression analysis, which separates normally distributed components of size-frequency samples (NORMSEP) using a maximum-likelihood approach (Gayanilo et al. 2002).

Results

Fish abundance and behavior—Fish could be observed within the profiling range of the hydroacoustic transducer during all deployments (Table 1). Although the fishes were more persistently distributed with densities below 1 m^{-3} during August and the beginning of September, they were observed to form dense shoals of up to 8 individuals per m^3 at the end of September and in October. These shoals were cruising continuously around the FAD. Compositions of the gill net catches (Table 2) reveal that the fish observed in the echograms are mainly perch *P. fluviatilis* L. and, to a lesser extent, ruffe *G. cernuus* (L.). By the end of September, the abundance of ruffe decreased, whereas perch abundance increased more than 10-fold. Hence, the dense fish shoals observed in late September and in October could be almost exclusively attributed to perch. The dominance of perch around the FAD was further confirmed by the video recordings and personal diving observations during the time period of investigation.

Length–frequency (*TL-F*) distributions are estimated for the two deployments on 08 October 2008, when highest fish abundances were observed in the net samples and hydroacoustic measurements (Fig. 2). NORMSEP analysis of the *TL-F* distributions of the net catches indicates the presence of three distinct size groups (SG) of perch with corresponding mean *TL* of 5.91, 8.07, and 10.46 cm (Fig. 2a). The comparison with the corresponding distribution derived from hydroacoustic measurements (Fig. 2b), however, indicates that the discrimination between mean *TL* of 8.06 and 10.46 cm is most likely a sampling artifact resulting from different gill net selectivity of the 9- and 12-mm mesh blade. Individuals with a *TL* of 9 cm may have not been caught well in either net blade and thus appear to be underrepresented in the gill net catches. According to the hydroacoustic *TL-F* distribution, three SG are classified by the NORMSEP routine (*TL* = 6.1 ± 0.5 cm, 9.0 ± 1.5 cm, and 14.2 ± 0.3 cm, mean ± SD, respectively).

The mean *TL* of SG1 and SG2 determined by the NORMSEP routine for the hydroacoustic data from 08 October 2008 and independently by analysis of variance (ANOVA) for net catches from 29 September 2008 and 08 October 2008 are in good agreement. The difference between the estimated mean *TL* in SG3 (Table 3) can be attributed to the low abundance of large fish (*TL* > 12 cm) so that a reliable fit to a normal distribution by the NORMSEP algorithm was not possible. Therefore the mean *TL* estimates of the ANOVA for the net catches were considered as more reliable than the NORMSEP estimate from the hydroacoustic data for SG3. The combination of data from net catches and hydroacoustic observations suggests the dominant occurrence of 0+ (mean *TL* = 6 cm), 1+ (mean *TL* = 9 cm), and, to a small proportion, also 2+ (and older) perch (mean *TL* = 12 cm) during our observations (Table 3). Swimming speeds estimated by SED tracking ranged from 0.02 to 1.09 m s^{-1} with a mean speed of 0.17 ± 0.13 m s^{-1} (SD).

Turbulence—TKE dissipation rates within individual profile segments varied between 10^{-6} and 10^{-11} W kg^{-1}. Strong variations were not only observed among different sampling days, but also within individual deployments and profiles (Fig. 3a). The range of values observed, as well as their high level of intermittency, are in accordance with other nearshore studies at Lake Constance (Lorke 2007) and cover the range of dissipation rates observed in lacustrine as well as in marine environments (Gregg and Sanford 1987; Imberger and Ivey 1991; Wüest and Lorke 2003).

On the basis of visual inspection of the echograms and video footage, individual microstructure profiles within one deployment were grouped and ensemble-averaged according to presence and absence of fish during profiling (Table 1). If fishes were present before but not during turbulence profiling, the respective cast was disregarded. As demonstrated in Fig. 3c,d, the classification into fish and no-fish profiles was particularly clear toward the end of the

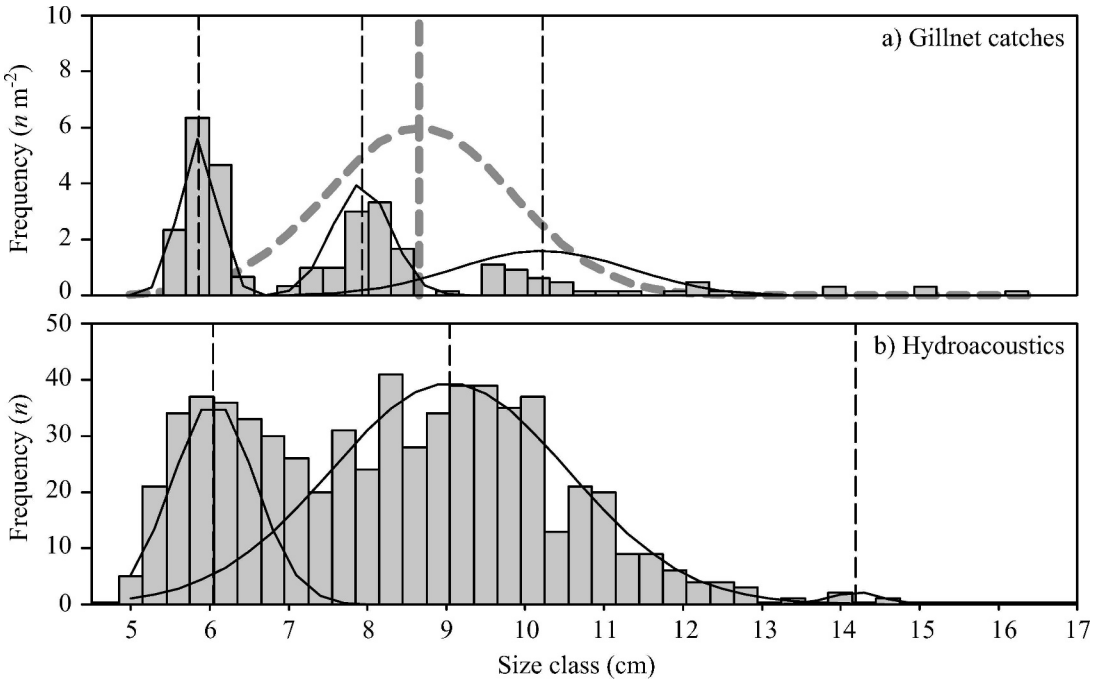

Fig. 2. Length–frequency (*TL-F*) distributions from 08 October 2008. (a) *TL-F*-distribution obtained from net catches for a total number of $n = 107$ fishes. (b) *TL-F* from hydroacoustic observations ($n = 670$). Solid lines encompass normally distributed size groups with mean lengths (vertical dashed lines) determined by a NORMSEP modal progression analysis. Whereas gill-net catches indicate the presence of two size groups at a mean *TL* of 8.07 and 10.46 cm, respectively, these size groups are considered to be the lower and upper ranges of an unimodal size group with a mean *TL* of 8.83 cm (gray dashed curve in panel a).

Table 3. Major size groups (SG), corresponding fish characteristics, and estimated production rates of mechanical energy. Total length *TL* (mean ± SD) is estimated by applying a maximum-likelihood approach (FISATII, Gayanilo et al. 2002) to the hydroacoustic data from 08 October 2008 ($TL_{NORMSEP}$) as well as by applying an ANOVA (TL_{ANOVA}) to catch data from 29 September 2008 and 08 October 2008. % is the relative abundance of SG at the respective sampling date. TL_M, WW_M, $\%_M$, N_{SG} are the corresponding mean values of length, weight, and relative and absolute abundances used in the following calculations. U_0 is the observed swimming speed and U_c is the cruising speed determined from WW_M using an empirical relationship provided by Huntley and Zhou (2004). *Re* is the Reynolds number (Eq. 4), P_{Drag} and P_{Shoal} are mean production rates of mechanical energy estimated (Eqs. 8 and 11, respectively) using the corresponding size–group-specific data provided in this table.

Parameter	SG1	SG2	SG3
$TL_{NORMSEP}$ (cm)	6.1(±0.5)	9.0(±1.5)	14.2(±0.3)
$TL_{ANOVA\ 29.09.2008}$ (cm)	5.9(±0.6)a	8.8(±1.0)b	12.3(±1.6)c
$TL_{ANOVA\ 08.10.2008}$ (cm)	6.0(±0.6)a	8.9(±1.0)b	11.9(±0.8)c
$\%_{29.09.2008}$*	32.3	61.4	6.2
$\%_{08.10.2008}$*	36.9	58.3	4.8
TL_M (cm)	6	9	12
WW_M (g)	2.1	7.2	22.5
$\%_M$	35	60	5
N_{SG} (m^{-3})	0.88	1.48	0.13
U_0 (m s^{-1})†	0.2	0.2	0.2
U_C (m s^{-1})	0.1	0.1	0.2
Re (-)	1.1×10^4	1.6×10^4	2.1×10^4
P_{Drag} (W kg^{-1})	6.5×10^{-8}	2.3×10^{-7}	3.3×10^{-8}
P_{Shoal} (W kg^{-1})	2.2×10^{-8}	7.5×10^{-8}	1.0×10^{-8}

a,b,c indicate homogenous groups determined by a two-way ANOVA including date and SG as predictors and a subsequent Tukey HSD test for unequal *n*.

* Relative proportions of SG to total abundance is not significantly different at both dates ($\chi^2 = 1.147$, df = 2, $p = 0.564$). Therefore $\%_M$ is determined by coarse interpolation of % between both dates.

† U_0 is not correlated with *TL* ($n = 1604$, $r^2 = 0.0001$, $p = 0.7752$); it is therefore estimated as the weighted mean (by no. of fish for each date) of all observations.

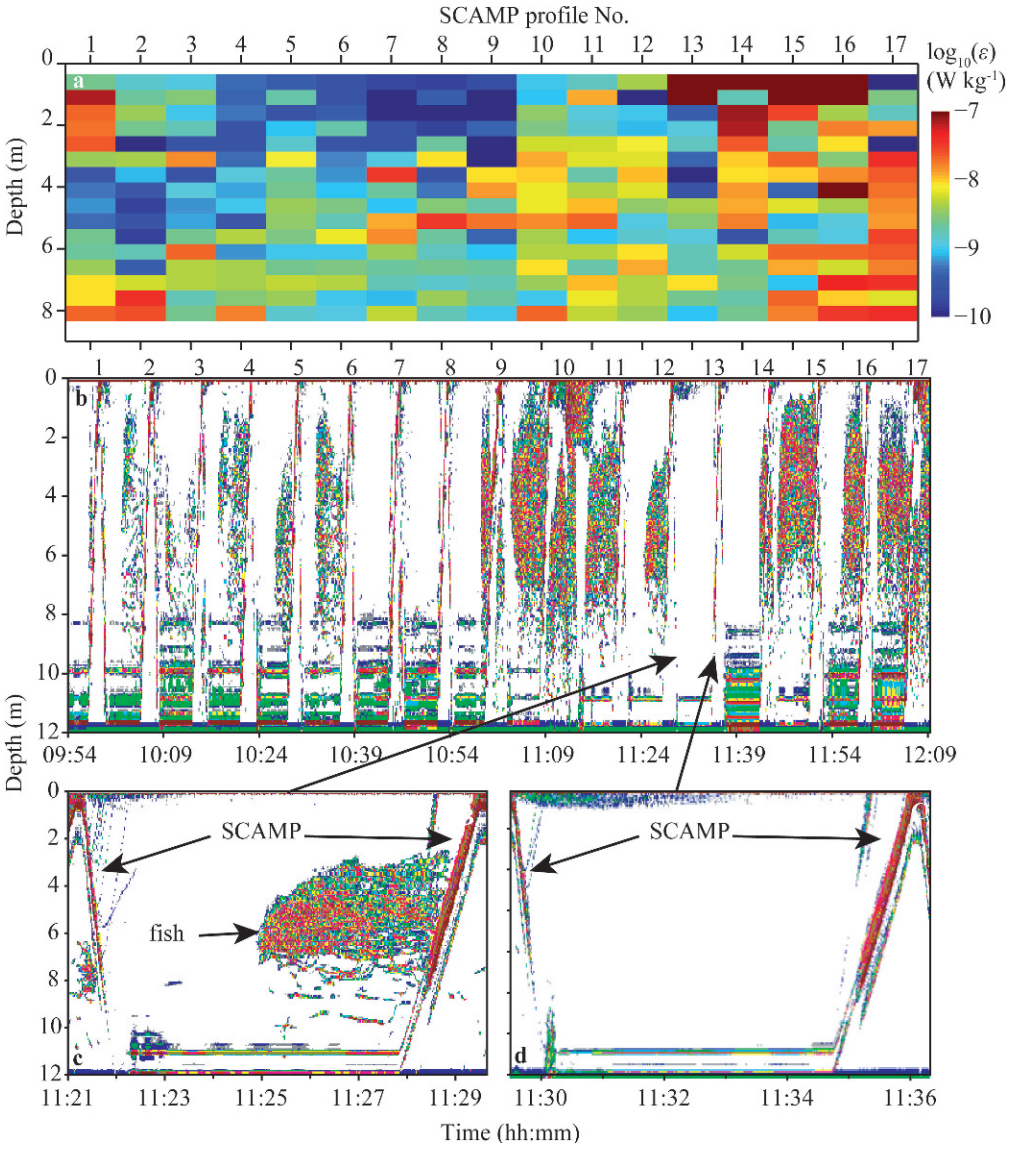

Fig. 3. Observations during the morning deployment on 08 October 2008. (a) Dissipation rates of turbulent kinetic energy ($\log_{10}[\varepsilon]$). The abscissa shows the profile number, which closely corresponds to the times shown in panel b. (b) Echogram of the entire deployment. The multiple green bars near the bottom represent the near field of the hydroacoustic transducer and interferences with the SCAMP profiler when it is held at its lower position in between profiling. The echogram shows 18 SCAMP releases toward the surface. After the ascent to the surface SCAMP was pulled to the lake bottom and rested there for 5 min before the next profile release. Numbers on top of the echogram refer to the respective profile numbers in panel a. (c) Details of SCAMP releases during presence and (d) absence of a fish shoal. The position of the two subsequently measured profiles within the deployment record is indicated by arrows. Turbulence measurements are conducted during the ascent of the profiler toward the end of the respective record. Estimated fish abundances are 4.7 and 0 m^{-3} in panels c and d, respectively.

measurement period, when fish were observed mainly in dense shoals. A still from the video recording during profiler ascent is exemplified in Fig. 4. Ensemble-averaged dissipation profiles for all deployments with fish densities exceeding 1 m^{-3} are shown in Fig. 5. Analysis of the deployments with such high abundances suggests that dissipation rates are enhanced when fishes are present in the profiling range. This effect was particularly observed during deployments and at depth ranges where background dissipation rates, here defined as ensemble-averaged dissipation rates in profiles where fishes were absent, were well below the range of dissipation rates observed when fishes were present.

The relation between the level of turbulence and the abundance of fish is analyzed by correlating depth-averaged dissipation rates estimated for each individual microstructure profile with the corresponding abundance of fish estimated from echo soundings during and immediately before the respective profile was measured (Fig. 6). The upper 2 m of the water column were excluded because of the influence of wind and waves. When applying a general linear model to the deployments with fish

Fig. 4. Still from the video recording during temperature microstructure profiling for the profile shown in Fig. 3c. The circular construction in the upper part of the picture is part of the sensor guard at the microstructure profiler.

abundances exceeding 1 m^{-3} (from 29 September 2008 until 08 October 2008), significant correlations between log-transformed dissipation rates, date, and fish abundance become evident, with an overall correlation coefficient of $r^2 = 0.79$ (Table 4). Furthermore, the model showed no significant relationship between log-transformed dissipation rates and the interaction between date and abundance, indicating that the slope of the linear regression between dissipation rate and abundance does not differ between sampling dates.

Data from deployments between 25 August 2008 and 11 September 2008 were not included into the statistical analysis, because during this period, the abundance of fish was very low (catch per unit effort < 1 fish h^{-1} m^{-2}). Furthermore, turbulence generated by fish shoals falls within the range indicated by the filled symbols in Fig. 6; therefore, they can only be detected by SCAMP if the level of background turbulence (produced by current shear and internal waves) is sufficiently low. However, the variation of background turbulence was usually within the range of fish-induced turbulence during August and the middle of September. Thus, no correlation between fish abundance and turbulence could be established for this period.

Turbulent mixing—Whereas TKE dissipation rates ε quantify the intensity of turbulent stirring, the resulting turbulent mixing can be described by the vertical turbulent diffusivity K_z. For stratified turbulence, K_z can be estimated by:

$$K_z = \gamma_{\mathrm{mix}} \frac{\varepsilon}{N^2} \tag{2}$$

where N is the buoyancy frequency describing vertical density stratification $\left[N^2 = (g/\rho)(\partial\rho/\partial z)\right]$ and γ_{mix} the mixing efficiency. Osborn (1980) estimated a maximum mixing efficiency of $\gamma_{\mathrm{mix}} < 0.2$. Although mixing efficiencies close to this maximum value were observed in numerous studies (Osborn 1980; Wolk and Lueck 2001;

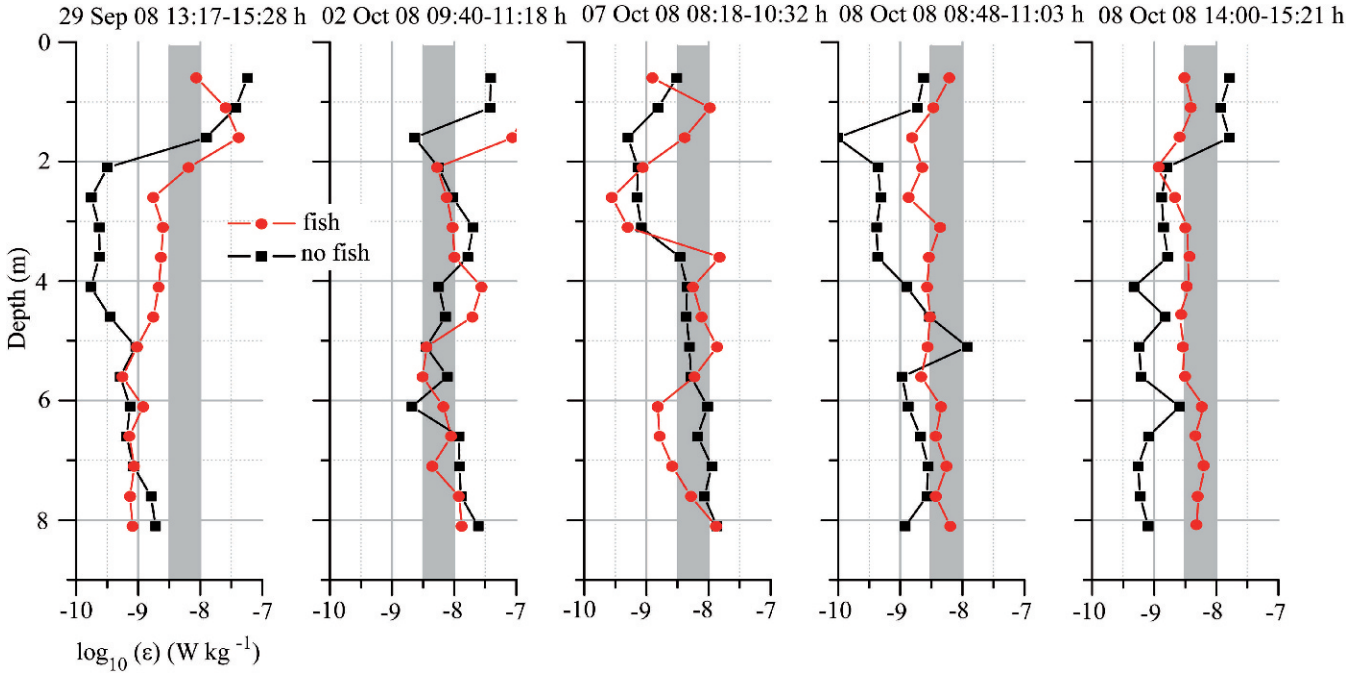

Fig. 5. Ensemble-averaged profiles of turbulent dissipation rates ε. Individual profiles measured during the particular deployment period indicated above each panel are grouped and averaged according to the presence and absence of fish in the echosounder at the respective profiling times. Only deployments with estimated abundances of fish exceeding 1 m^{-3} are considered (Table 1). The same axis scaling is used for each plot; gray bars encompass the typical range of dissipation rates observed during the presence of fish (3×10^{-9} W $kg^{-1} < \varepsilon < 1 \times 10^{-8}$ W kg^{-1}).

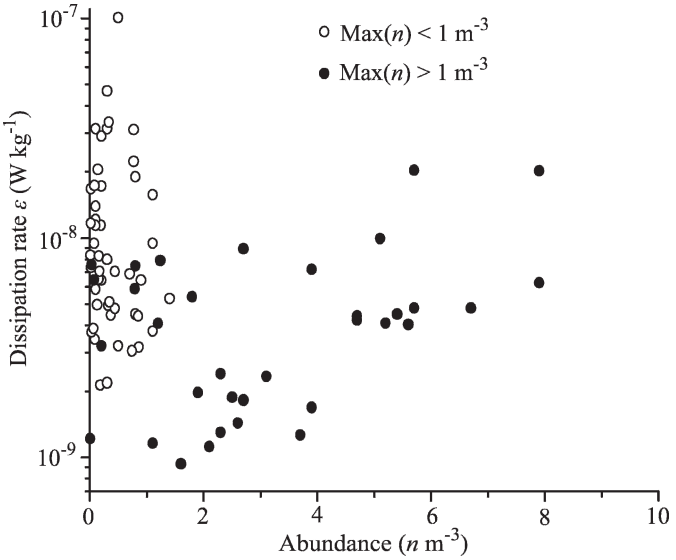

Fig. 6. Depth-averaged dissipation rates of turbulent kinetic energy vs. fish abundance observed during or immediately before profiling. Filled symbols are used for deployments with maximum observed fish densities exceeding 1 m^{-3} (29 September 2009 and later).

Wüest and Lorke 2009), there is growing evidence that γ_{mix} can be much smaller than 0.2 (Ivey et al. 2008), particularly in biologically induced turbulence (Visser 2007*a*; Gregg and Horne 2009).

Depth- and ensemble-averaged mixing efficiencies in profiles with and without fish were estimated from Eq. 2 by replacing K_z with an estimate of the turbulent diffusivity obtained from a steady-state balance of production and dissipation of temperature variance in turbulent flow (Osborn and Cox 1972):

$$\gamma_{mix} = \frac{1}{2}\frac{\chi_T N^2}{\varepsilon}\left(\frac{\partial \overline{T}}{\partial z}\right)^{-2} \quad (3)$$

where χ_T is the dissipation rate of temperature variance and $\partial \overline{T}/\partial z$ the vertical gradient of mean temperature (e.g., Wain and Rehmann 2005). Observed values of γ_{mix} did not differ between profiles with fish (γ_{mix} = 0.22) and without fish (γ_{mix} = 0.21) and no correlation was observed between γ_{mix} and fish abundance.

Discussion

Biomechanical constraints for turbulence production by swimming fish—Whether fish swimming is associated with strictly laminar flow or with the production of turbulent eddies can be analyzed in terms of the Reynolds number *Re*

$$Re = \frac{U_0 TL}{\nu} \quad (4)$$

where U_0 is the characteristic velocity scale (swimming velocity), *TL* a characteristic length scale (fish size), and ν the kinematic velocity of water ($\nu \approx 1 \times 10^{-6}$ m^2 s^{-1}). Although the critical value of *Re*, at which the transition from laminar to turbulent flow occurs, depends on the particular geometry of the flow, values in the range of $Re \approx 0.5–2 \times 10^4$ estimated for our observations (Table 3) indicate turbulent flow. Huntley and Zhou (2004) provided a set of empirical formulas relating Reynolds number of animal swimming to body mass, size, and swimming speed by analyzing data from 100 marine species. Our measurements fit surprisingly well into this analysis, as exemplified by the close agreement between the cruising speed U_c, estimated solely from body mass, and observed swimming speed U_0 (Table 3).

Table 4. Results of a general linear model (GLM) applied to the observed depth-averaged log-dissipation rates on 29 September 2008, 02 October 2008, 07 October 2008, and 08 October 2008. Date and fish abundance were used as categorical and continuous predictors in the GLM. Date × abundance indicates the interactive influence of both predictors for which a lack of significance does not suggest any difference in the slope of the linear relationship between fish abundance and log-dissipation (Fig. 6). *F* is the resulting value of the *F*-statistics and *p* the level of significance. The multiple r^2 of the GLM was 0.79 and was highly significant (total $n = 61$, $p < 0.001$).

Factor	*F*	*p*
Date	37.87	<0.001
Abundance	11.39	0.001
Date×abundance	1.02	0.391

Following Huntley and Zhou (2004), the production rate of mechanical energy P_{Drag} by swimming fish with an abundance N (m^{-3}) is the product of swimming speed and the work each fish does to overcome the drag force *D*:

$$P_{Drag} = \frac{N}{\rho} U_0 D \quad (5)$$

where density of water ρ is used to express P_{Drag} in units of power per unit mass of water (W kg^{-1}). In turbulent flows *D* can be estimated as

$$D = \frac{1}{2}\rho {U_0}^2 A_w C_D \quad (6)$$

with A_w being the wetted surface area and C_D the drag coefficient. C_D can be approximated by that of an ideal flat plate parallel to the flow, for which the theoretical drag coefficient is given as:

$$C_D = 0.072\, Re^{-0.2} \quad (7)$$

Actual measuremnts of C_D indicate that animal body shapes are less than ideal in this respect, so Eq. 7 yields a conservative estimate (Huntley and Zhou 2004). Hence, P_{Drag} can be estimated by combining Eqs. 4 to 7 and by approximating A_w as 2*TLH*, where the body height is estimated as *TL*/3:

$$P_{Drag} = \frac{0.072}{3} N\, {U_0}^{14/5}\, TL^{9/5}\, \nu^{0.2} \quad (8)$$

Estimates of P_{Drag} for the three distinct size groups and for mean fish abundances observed in our measurements vary

between 3×10^{-8} and 2×10^{-7} W kg^{-1} (Table 3) and highest production rates are contributed by the most abundant size group ($TL = 9$ cm).

Bioenergetic constraints for turbulence production by swimming fish—Alternatively, the production rate of TKE by swimming fish can be estimated from a metabolic point of view. Using an empirical analysis of numerous published data sets, Boisclair and Tang (1993) found the following relationship between the metabolic cost of routine swimming of an individual fish O_h (mg O_2 h^{-1}), fish weight (W; g wet), and swimming speed (U_0; cm s^{-1}):

$$O_h = 0.117 W^{0.54} {U_0}^{1.09} \quad (9)$$

Energy equivalents of these metabolic costs can be estimated using an oxycaloric value of 13.6 J (mg O_2)$^{-1}$ (Elliot and Davison 1975; Rennie et al. 2005). Hence, Eq. 9 can be written as:

$$E_{aerob} = 4.4 \cdot 10^{-4} W^{0.54} {U_0}^{1.09} \quad (10)$$

where E_{aerob} is the metabolic power (W) spent by one fish for swimming. To estimate the production rate of mechanical energy generated per unit mass of water P_{Shoal} (W kg^{-1}), the abundance N, water density ρ, as well as the propulsive efficiency η must be taken into account:

$$P_{Shoal} = \frac{\eta N}{\rho} E_{aerob} \quad (11)$$

Although η can vary significantly among species, an estimate can be obtained from:

$$\eta = 0.39 {U_0}^{0.24} \quad (12)$$

(U_0 in m s^{-1}, Wardle et al. 1996), resulting in $\eta \approx 0.26$ for our observations. Estimates of P_{Shoal} for the mean fish abundances observed in the three distinct size groups in our measurements vary between 1×10^{-8} and 7×10^{-8} W kg^{-1} (Table 3).

Comparison with observations—For low levels of background turbulence and for fish abundances exceeding 1 m^{-3} we have observed a significant correlation between both variables (Table 4), indicating that water column turbulence increases with increasing fish abundance. The range of turbulence dissipation rates for which the correlation is observed (10^{-9}–10^{-8} W kg^{-1}), however, overlaps frequently with the range of dissipation rates generated by current shear due to wind-forcing and internal waves (Wüest and Lorke 2003; Lorke 2007). The latter fact explains why this correlation could only be observed in a limited number of our deployments, i.e., only if fish abundance was exceeding about 1 m^{-3} and background turbulence was sufficiently weak. The observed correlation clearly demonstrates that biologically produced turbulence, due to swimming fish in shoals, can contribute to water column turbulence at a similar magnitude as physically produced turbulence does. This result was found for the range of observed TKE dissipation rates as well as for depth- and ensemble-averaged values.

This conclusion is further confirmed by the two different estimates of the production rate of TKE by swimming fish, on the basis of a biomechanical (P_{Drag}) and on the basis of a metabolic (P_{Shoal}) approach (Table 3). Although the two estimates differ by a factor of three ($P_{Shoal} \approx 3P_{Drag}$), this difference is not surprising, considering the broad range of aquatic biota using different types of locomotion on which the underlying empirical relationships are based. More surprisingly, both calculated production rates of mechanical energy are about two orders of magnitude higher than the observed dissipation rates of turbulence. There are two reasons why the estimated production rates should be considerably greater than the dissipation rates: First, both estimates consider the total mechanical energy produced by swimming fish, but only the turbulent energy, dissipated in overturning eddies, is measured by the microstructure profiler. Some unknown fraction of the total mechanical energy is dissipated by skin friction within the viscous sublayer surrounding the fish, without being cascaded through turbulent eddies. Second, and probably more important, a steady-state balance between production and dissipation can only be expected for homogenous turbulence, whereas the major part of the fish-generated energy is produced very locally, within the boundary layer and in the wake of individual fish (Anderson et al. 2001). It can be expected that the fish do not saturate the fluid with their turbulence and that local production rates, and hence the local intensities of turbulence around the fish, are much higher than the dissipation rates estimated from temperature microstructure averaged over 0.5-m-long profile segments. Unfortunately, the inherent statistical nature of turbulence and particularly its strong dynamics in environmental systems do not allow for locally resolved dissipation estimates with sufficient significance under field conditions.

Vertically averaged dissipation rates can be considered as a bulk parameter describing vertical mixing (Eq. 2). Our measurements do not indicate significantly reduced mixing efficiencies within fish aggregations and the values observed ($\gamma_{mix} \approx 0.2$) are in close agreement with those typically found in stratified water bodies (Ivey et al. 2008). Gregg and Horne (2009), in contrast, observed a reduction of mixing efficiencies within aggregations of marine animals to values of about 1% of this value. Although the size, species composition, and abundance of the animals were not sampled directly by these authors, TKE dissipation rates, exceeding our observations by a factor of 100, indicate a much higher contribution of biologically generated turbulence to overall turbulent stirring. This could potentially be caused by higher abundance or swimming speed, or larger size of the animals. Following Visser (2007*a*), it can be expected that the mixing efficiency is decreasing with an increasing contribution of turbulence generated by individual movements of small animals to overall turbulent stirring.

On the basis of our observations, it can be hypothesized that biologically produced turbulence by swimming fish aggregated in shoals contributes significantly to vertical mixing around the FAD, at least during time periods of weak levels of shear-generated background turbulence. To what extent this additional mixing and the corresponding

vertical fluxes of nutrients and dissolved gases affect the local ecosystem around the artificial structure requires more comprehensive measurements. Also the questions of whether the seasonally recurring aggregation of young-of-the-year fish is influenced by water column turbulence, or by the additional turbulence generated by shoaling, remain unanswered. Future studies, aiming at closing the gap between observed and empirically predicted turbulence dissipation and production rates, will help to answer such question and thus provide a key for understanding the role of biologically generated turbulence in aquatic ecosystems.

Acknowledgments

Reiner Eckmann provided the hydroacoustic and fishing equipment and Miriam Ritter assisted during microstructure profiler measurements and echosounder calibration. The scientific diving group at the University of Konstanz installed and retrieved the experimental setup. Earlier drafts of the manuscript were improved by the helpful comments of two anonymous reviewers and the associate editor.

This work was financially supported by a Young Scholar Fund research grant of the University of Konstanz and the German Research Foundation (DFG).

References

Allouche, S., and P. Gaudin. 2001. Effects of avian predation threat, water flow and cover on growth and habitat use by chub, *Leuciscus cephalus*, in an experimental stream. Oikos **94:** 481–492.

Anderson, E. J., W. R. McGillis, and M. A. Grosenbaugh. 2001. The boundary layer of swimming fish. J. Exp. Biol. **204:** 81–102.

Balk, H., and T. Lindem. 2006. SONAR5_Pro. University of Oslo. Available from http://www.fys.uio.no/~hbalk/sonar4_5/Downloads.htm

Bassett, C. E. 1994. Use and evaluation of fish habitat structures in lakes of the eastern United States by the USDA forest service. Bull. Mar. Sci. **55:** 1137–1148.

Batchelor, G. K. 1959. Small-scale variation of convected quantities like temperature in turbulent fluid. J. Fluid Mech. **5:** 113–133.

Behrmann-Godel, J., G. Gerlach, and R. Eckmann. 2006. Kin and population recognition in sympatric Lake Constance perch (*Perca fluviatilis* L.): Can assortative shoaling drive population divergence? Behav. Ecol. Sociobiol. **59:** 461–468.

Boisclair, D., and M. Tang. 1993. Empirical analysis of the influence of swimming pattern on the net energetic cost of swimming fish. J. Fish Biol. **42:** 169–183.

Cech, M., and J. Kubecka. 2002. Sinusoidal cycling swimming pattern of reservoir fishes. J. Fish Biol. **61:** 465–471.

Dewar, W. K., R. J. Bingham, R. L. Iverson, D. P. Nowacek, L. C. St. Laurent, and P. H. Wiebe. 2006. Does the marine biosphere mix the ocean? J. Mar. Res. **64:** 541–561.

Drucker, E. G., and G. V. Lauder. 2002. Experimental hydrodynamics of fish locomotion: Functional insights from wake visualizations. Integr. Comp. Biol. **42:** 243–257.

Elliot, J. M., and W. Davison. 1975. Energy equivalents of oxygen consumption in animal energetics. Oecologia **19:** 195–201.

Enders, E. C., D. Boisclair, and A. G. Roy. 2003. The effect of turbulence on the cost of swimming for juvenile Atlantic salmon (*Salmo salar*). Can. J. Fish. Aquat. Sci. **60:** 1149–1160.

Fischer, P., and R. Eckmann. 1997. Seasonal changes in fish abundance, biomass and species richness in the littoral zone of a large European lake, Lake Constance, Germany. Arch. Hydrobiol. **139:** 433–448.

Gayanilo, F. C., P. Sparre, and D. Pauly. 2002. FISAT II User's guide. Food and Agricultural Organisation of the United Nations. Available from http://www.fao.org/fi/statist/fisoft/fisat/index.htm

Gregg, M. C., and J. K. Horne. 2009. Turbulence, acoustic backscatter, and pelagic nekton in Monterey Bay. J. Phys. Oceanogr. **39:** 1077–1096.

———, and T. B. Sanford. 1987. Shear and turbulence in thermohaline staircases. Deep-Sea Res. **34:** 1689–1696.

Hoare, D. J., G. D. Ruxton, J.-G. J. Godin, and J. Krause. 2000. The social organization of free-ranging fish shoals. Oikos **89:** 546–554.

Hondzo, M., and Z. Haider. 2004. Boundary mixing in a small stratified lake. Water Resour. Res. **40:** W03101, doi:10.1029/2002WR001851.

Huntley, M. E., and M. Zhou. 2004. Influence of animals on turbulence in the sea. Mar. Ecol. Prog. Ser. **273:** 65–79.

Imberger, J., and G. N. Ivey. 1991. On the nature of turbulence in a stratified fluid. Part II: Application to lakes. J. Phys. Oceanogr. **21:** 659–680.

Ivey, G. N., K. B. Winters, and J. R. Koseff. 2008. Density stratification, turbulence, but how much mixing? Annu. Rev. Fluid Mech. **40:** 169–184.

Kunze, E., J. F. Dower, I. Beveridge, R. K. Dewey, and K. P. Bartlett. 2006. Observations of biologically generated turbulence in a coastal inlet. Science **313:** 1768–1770.

———, ———, R. K. Dewey, and E. A. D'asaro. 2007. Mixing it up with krill. Science **318:** 1239.

Lewis, D. M., and T. J. Pedley. 2001. The infuence of turbulence on plankton predation strategies. J. Theor. Biol. **210:** 347–365.

Liao, J. C. 2007. A review of fish swimming mechanics and behaviour in altered flows. Phil. Trans. R. Soc. Lond. B Biol. Sci. **362:** 1973–1993.

Löffler, H. 1997. Artificial habitats for fishes in Lake Constance (Bodensee): Observation of fish aggregating devices with a remotely operated vehicle. Fish. Manag. Ecol. **4:** 419–420.

Lorke, A. 2007. Boundary mixing in the thermocline of a large lake. J. Geophys. Res. **112:** C09019, doi:10.1029/2006JC004008.

———, B. Müller, M. Maerki, and A. Wüest. 2003. Breathing sediments: The control of diffusive transport across the sediment–water interface by periodic boundary-layer turbulence. Limnol. Oceanogr. **48:** 2077–2085.

———, A. Weber, H. Hofmann, and F. Peeters. 2008. Opposing diel migration of fish and zooplankton in the littoral zone of a large lake. Hydrobiologia **600:** 139–146, doi:10.1007/s10750-007-9183-1.

Mackenzie, B. 2000. Turbulence, larval fish ecology and fisheries recruitment: A review of field studies. Oceanol. Acta **23:** 357–375.

Mürle, U., J. Ortlepp, and P. Rey. 2004. Lake Constance: Condition, facts and perspectives, 2nd ed. Internationale Gewässerschutzkommission für den Bodensee (IGKB). [In German.]

Neumann, E., G. Thoresson, and A. Sandström. 1996. Swimming activity of perch *Perca fluviatilis* in relation to temperature, day-length and consumption. Ann. Zool. Fenn. **33:** 669–678.

Nikora, V. I., J. Aberle, B. J. F. Biggs, I. G. Jowett, and J. R. E. Sykes. 2003. Effect of fish size, time-to-fatigue, and turbulence on swimming performance: A case study of *Galaxias maculatus*. J. Fish Biol. **63:** 1365–1382.

Osborn, T. R. 1980. Estimates of the local rate of vertical diffusion from dissipation measurements. J. Phys. Oceanogr. **10:** 83–89.

———, and C. S. Cox. 1972. Oceanic fine structure. Geophys. Fluid Dyn. **3:** 321–345.

Pitchford, J. W., A. James, and J. Brindley. 2003. Optimal foraging in patchy turbulent environments. Mar. Ecol. Prog. Ser. **256:** 99–110.

Prince, E. D., and O. E. Maughan. 1978. Freshwater artificial reefs: Biology and economics. Fisheries **3:** 5–9.

Rennie, M. D., N. C. Collins, B. J. Shuter, J. W. Rajotte, and P. Couture. 2005. A comparison of methods for estimating activity costs of wild fish populations: More active fish observed to grow slower? Can. J. Fish. Aquat. Sci. **62:** 767–780.

Reyjol, Y., P. Fischer, S. Lek, R. Rösch, and R. Eckmann. 2005. Studying the spatiotemporal variation of the littoral fish community in a large prealpine lake, using self-organizing mapping. Can. J. Fish. Aquat. Sci. **62:** 2294–2302.

Rogers, K. B., and E. P. Bergersen. 1999. Utility of synthetic structures for concentrating adult northern pike and largemouth bass. N. Am. J. Fish. Manage. **19:** 1054–1065.

Ruddick, B., A. Anis, and K. Thompson. 2000. Maximum likelihood spectral fitting: The Batchelor spectrum. J. Atmos. Ocean. Technol. **17:** 1541–1555.

Schmidt-Nielsen, K. 1997. Animal physiology—adaptation and environment, 5th ed. Cambridge Univ. Press.

Simmonds, J., and D. N. Maclennan. 2005. Fisheries acoustics—theory and practice, 2nd ed. Blackwell.

Stoll, S., P. Fischer, P. Klahold, N. Scheifhacken, H. Hofmann, and K.-O. Rothhaupt. 2008. Effects of water depth and hydrodynamics on the growth and distribution of juvenile cyprinids in the littoral zone of a large prealpine lake. J. Fish Biol. **72:** 1001–1022.

Triantafyllou, M. S., G. S. Triantafyllou, and D. K. P. Yue. 2000. Hydrodynamics of fishlike swimming. Annu. Rev. Fluid Mech. **32:** 33–53.

Visser, A. W. 2007*a*. Biomixing of the oceans? Science **316:** 838–839.

———. 2007*b*. Mixing it up with krill—response. Science **318:** 1239–1239.

Wain, D. J., and C. R. Rehmann. 2005. Eddy diffusivity near bubble plumes. Water Resour. Res. **41:** W09409, doi: 10.1029/2004WR003896.

Wang, N., and R. Eckmann. 1994. Distribution of perch (*Perca fluviatilis* L.) during their first year of life in Lake Constance. Hydrobiologia **277:** 135–143.

Wardle, C. S., N. M. Soofiani, F. G. O'Neill, C. W. Glass, and A. D. F. Johnston. 1996. Measurements of aerobic metabolism of a school of horse mackerel at different swimming speeds. J. Fish Biol. **49:** 854–862.

Wolk, F., and R. G. Lueck. 2001. Heat flux and mixing efficiency in the surface mixing layer. J. Geophys. Res. **106:** 19547–19562.

Wüest, A., and A. Lorke. 2003. Small-scale hydrodynamics in lakes. Annu. Rev. Fluid Mech. **35:** 373–412.

———, and ———. 2009. Small-scale turbulence and mixing: Energy fluxes in stratified lakes, p. 628–635. *In* G. E. Likens [ed.], Encyclopedia of inland waters. Academic.

Associate editor: Chris Rehmann

Received: 31 March 2009
Accepted: 13 October 2009
Amended: 13 October 2009